Available online at www.sciencedirect.com
ScienceDirect
Journal of Power Sources 172 (2007) 2–13
JOURNAL OF POWER SOURCES
www.elsevier.com/locate/jpowsour

Membrane resistance and current distribution measurements under various operating conditions in a polymer electrolyte fuel cell

D.J.L. Brett [a], S. Atkins [b], N.P. Brandon [c], N. Vasileiadis [a], V. Vesovic [c], A.R. Kucernak [b,*]

[a] *Department of Chemical Engineering, Imperial College London, London SW7 2AZ, UK*
[b] *Department of Chemistry, Imperial College London, London SW7 2AZ, UK*
[c] *Earth Science and Engineering, Imperial College London, London SW7 2AZ, UK*

Received 22 November 2006; received in revised form 14 May 2007; accepted 16 May 2007
Available online 25 May 2007

Abstract

The ability to make spatially resolved measurements in a fuel cell provides one of the most useful ways in which to monitor and optimise their performance. Localised membrane resistance and current density measurements for a single channel polymer electrolyte fuel cell are presented for a range of operating conditions. The current density distribution results are compared with an analytical model that exhibited generally good agreement across a broad range of operating conditions. However, under conditions of high air flow rate, an increase in current is observed along the channel which is not predicted by the model. Under such circumstances, localised electrochemical impedance measurements show a decrease in membrane resistance along the channel. This phenomenon is attributed to drying of the electrolyte at the start of the channel and is more pronounced with increasing operating temperature.

Under conditions of reactant depletion, an increase in electrolyte resistance with decreasing current is observed. This is due to the hydrating effect of product water and electro-osmotic drag through the membrane when ionic current is flowing. Localised conduction is shown to be an effective means of conditioning previously unused membrane electrode assemblies by forcing passage of ionic current through the electrolyte.

Keywords: Polymer electrolyte fuel cell; Current distribution; Membrane resistance distribution; Humidification; Water management; Preconditioning

1. Introduction

The polymer electrolyte fuel cell (PEFC) is an electrochemical energy conversion device with characteristics that make it a promising technology as a replacement for the internal combustion engine and as the power source for mobile electronic devices [1]. To emerge and be successful, the PEFC must be able to deliver equivalent or superior performance to the incumbent technology at a comparable price. Reaching the targets set for durability, power density and cost involves overcoming numerous technical hurdles, many of which relate to the membrane electrolyte. The role of the membrane electrolyte is to allow proton conduction from the anode to the cathode, while having the properties of an electronic insulator and acting as a barrier to reactant crossover. These requirements are fulfilled by a remarkable class of polymer, exemplified by DuPont's Nafion®. Although many alternative polymeric materials have been developed, some with claimed superior performance, perfluorinated sulphonic acid polymers represent the membrane material of choice for most membrane electrode assembly (MEA) manufacturers. The generic structure is based on a hydrophobic perfluoronated polymer backbone with perfluoronated sidechains that are terminated by a hydrophilic sulphonic acid group. The exact mechanism of proton transport through the membrane is complex and not fully understood; to conduct protons the material must be hydrated and the ionic conductivity is a nonlinear function of water content [2,3]. Various mechanisms of proton conduction through the membrane have been proposed [4–6], although none account for all of the phenomena measured experimentally. Whatever the exact transport mechanism, the requirement that the membrane should be hydrated is crucial in obtaining optimum performance. Understanding water management and achieving adequate hydration of the membrane is a significant technical problem facing fuel cell developers.

* Corresponding author. Tel.: +44 20 75945831; fax: +44 20 75945804.
E-mail address: a.kucernak@imperial.ac.uk (A.R. Kucernak).

0378-7753/$ – see front matter © 2007 Elsevier B.V. All rights reserved.
doi:10.1016/j.jpowsour.2007.05.071

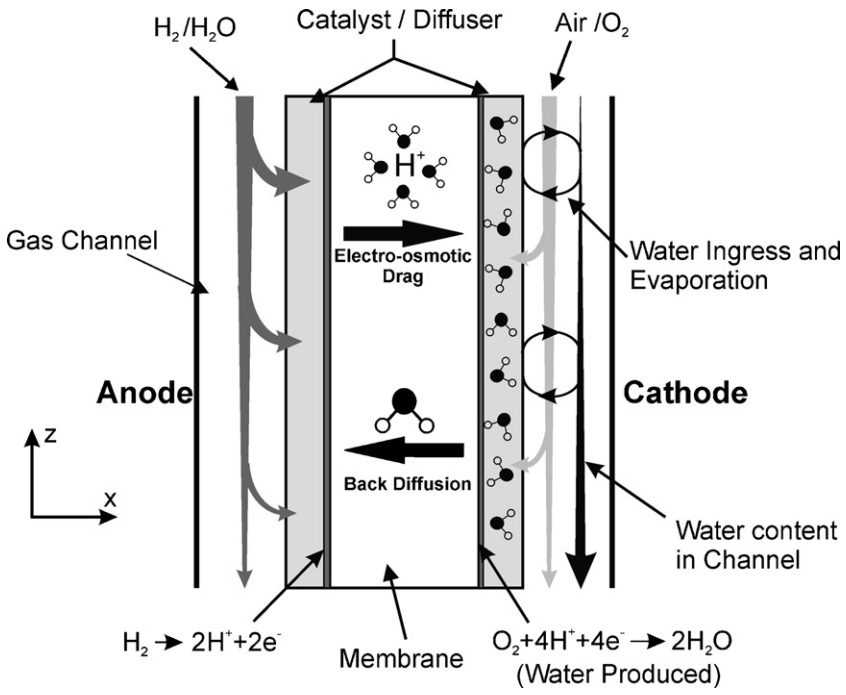

Fig. 1. Illustration of the various water transport mechanisms existing within PEFCs.

Fig. 1 illustrates the various mechanisms of water transported around the fuel cell. The graphic depicts a cross-section through a single cell fed with humidified hydrogen at the anode and dry air (or oxygen) at the cathode. The hydrogen reacts at the anode catalyst and produces protons which travel through the membrane accompanied by a number of water molecules in a process of electro-osmotic drag. The flux of water transported in this fashion is dependant on the number of water molecules associated with each proton (the drag coefficient) and the ionic current density. Protons arriving at the cathode react with oxygen to produce water. This results in water being produced at, and delivered to, the cathode; while at the anode it is being depleted. This is one reason for preferential humidification of the anode reactant stream. However, the water at the cathode can be transported back to the anode via diffusion driven by the concentration gradient or by convection due to an applied pressure differential between the anode and cathode. This water flux can be represented by the following equation [7].

$$J_{H_2O} = \lambda_{drag}\frac{j}{F} - D_w\frac{dc_w}{dx} - c_w\frac{k_p}{\mu}\frac{dP_w}{dx} \quad (1)$$

where J_{H_2O} is the flux of water through the membrane from the anode side to the cathode side, j the current density, F the Faraday's constant, D_w the diffusion coefficient of water through the membrane, c_w the concentration of water in the membrane, k_p the hydraulic permeability of water in the membrane, μ the viscosity of water in the membrane, P_w the hydrostatic pressure of water in the membrane and x is the dimension through the plane of the membrane.

The electro-osmotic effect results in the transfer of water from anode to cathode provided that ionic current is flowing; however, the relative amount of water transferred will change due to the drag coefficient's dependence on the level of hydration of the membrane [8] and temperature [9]. In contrast, back diffusion and convection may, in principle, be in either direction. Thus, the net flux, J_{H_2O}, may also be in either direction (anode to cathode or cathode to anode) depending upon the magnitude of each of the terms. Furthermore, as local conditions within a fuel cell vary with position (e.g. temperature, reactant concentration, local current density, water vapour pressure), J_{H_2O} may vary with position within a fuel cell. For example, if a channel is fed with dry air at the cathode and well-hydrated hydrogen at the anode, net water transport may be from anode to cathode at the start of the channel, but in the opposite direction once the gas in the cathode channel becomes hydrated with product water [7]. The model of Bernardi and Verbrugge [10], predicts that net water flow can occur in the direction of the cathode or the anode depending on conditions such as current density and pressure difference between anode and cathode. Indeed, different parts of the same electrode can have water flow in different directions [11,12].

Dehydration of the electrolyte membrane degrades performance; however, a surplus of water can also lead to problems. Excess water can block pores in the catalyst layer and gas diffusion layer (GDL) and lead to 'flooding' which impedes reactant transport. In this case, external hydration of the reactant gas may actually be a detriment to performance. Thus, an understanding of the way in which the local conditions affect water transport within a fuel cell is important in realising optimal performance.

In addition to water transport through the membrane, lateral transport of water through the flow-field (i.e. in the z direction specified in Fig. 1) is a factor to be considered. Convection of water through the gas channels and gas diffusion layer will be the main driving force for this process. Water can be lost

from the membrane into the gas stream only to be absorbed by the membrane further along the channel. This has the effect of redistributing water to different parts of the cell. Other factors that determine the extent of hydration of the membrane include: temperature, current density, flow plate design and reactant flow rate. To complicate matters further, these factors are spatially variant.

Direct methods of quantifying the flow and balance of water in a fuel cell system have normally been limited to condensation of exhaust [10,13,14] or positioning of humidity sensors [15]. However, the water content of the membrane electrolyte is typically inferred from ionic resistance measurements.

Numerous numerical models have been presented that endeavour to describe the operation of PEFCs, many of which consider the role of water [8,16–19]. The findings in these papers point to the profound impact that water has on the way a fuel cell operates. As insightful and elegant as these models may be, what they attempt to achieve is ambitious considering the number of factors, and the extent of coupling between these factors, that must be considered if the model is to operate successfully. Only by direct measurement of current and membrane resistance can these models be tested and improved. Methods that utilise spatially resolved measurements are one of the best ways to achieve this.

1.1. Measurement of current density distribution and membrane resistance in a PEFC

From the preceding overview, it is clear that water management is a crucial issue in determining PEFC performance. The electrolyte accounts for the majority of the internal resistance of the MEA and it is vital that it remains adequately hydrated. Various methods have been used to measure membrane ionic resistance, both in working fuel cells and ex situ, and in the through-plane and in-plane directions. Examples of these include: current interrupt [20], current pulse [21], coaxial probe [22], the Guillou's cell [23], mercury cell [23], LMEI clip [23], dc methods [24,25] and the most widely used technique—electrochemical impedance spectroscopy (EIS) [26–29]. Amongst published results, there is some disagreement between membrane resistance values measured by different techniques on the same material. Slade et al. present a review of membrane resistance measurements, and tabulate some of the values reported in the literature [30]. The main reason for the disparity in these values is that a range of factors that are known to affect membrane resistance are not fixed or controlled accurately, e.g. temperature, membrane thickness, equivalent weight, humidification, liquid/electrolyte immersion and pre-treatment. As most measurements are performed on bulk samples, they will be insensitive to any spatial variation in the properties of the membrane. However, this will not emulate the conditions present in a working fuel cell, where membrane properties, reactant and current distribution vary temporally and spatially.

Localised current density measurements are a powerful means of monitoring fuel cell performance. A range of current distribution techniques have been applied to PEFCs [31–38]. Current density mapping can be adapted for the measurement of localised electrochemical impedance spectroscopy (LEIS) and localised voltammetry measurements [39–42]. The LEIS technique reported previously [40] concentrated on the low frequency features of the EIS response associated with reactant mass transport; it was found that certain operating conditions led to a distribution of impedance response due to reactant depletion in the channel. These results indicated that care is necessary when interpreting 'whole-cell' EIS measurements performed on a fuel cell operating at low stoichiometries (specifically, $\lambda < 2$). The work presented here focuses on the high frequency 'real' impedance response, and uses this parameter to measure the spatial variation of membrane resistance under different conditions inside a working PEFC.

Only a modest amount of work has been presented that considers membrane resistance distribution. Noponen et al. used the current interruption method on a segmented current collector under the condition of a flow pulse to derive the local resistance of the cell [43]. It was reasoned that when a cell is subjected to an over-stoichiometric pulse of reactant, the concentration variation of reactant is equalised and all variation in the current distribution is due to the localised resistance of the membrane. The results implied that a higher resistance, observed close to the reactant inlet, is due to the drying effect of unhumidified hydrogen. Büchi and Scherer used an auxiliary current pulse method to measure membrane resistance at the gas-inlet and gas-outlet of a fuel cell [44]. The results imply that inadequate external hydration leads to complex in-plane patterns of membrane hydration. Cleghorn et al. [32] applied a similar method to that reported herein to study a 2D flow-field. The results identified variation in resistance due to dehydration of the membrane and highlighted the effect of internal humidification and inadequate external humidification on the distribution of current and resistance.

Application of EIS to the study of fuel cells is well established. Work by Springer et al. [26], for instance, has built a framework of knowledge from which rational interpretation of EIS results can be made. It is generally accepted that certain features of a typical impedance response can be attributed to specific parameters. The point at which the impedance response crosses the real axis at high frequency, is taken as a measure of the internal Ohmic resistance of the system. This component can be considered as a linear combination of the following resistances:

$$R_{\text{Total}} = R_{\text{Connect}} + R_{\text{Contact}} + R_{\text{MEA}} \quad (2)$$

where R_{Connect} represents the electronic resistance of the leads and connections from the fuel cell to the load or test device, including the current collector plates; R_{Contact} the contact resistance between the plate and GDL on both sides of the cell; R_{MEA} constitutes the electronic through-plane resistance of the GDL, the ionic resistance of the membrane and the mixed electronic and ionic resistance of the GDL/catalyst/membrane interface.

The measurement technique used in this study allows the R_{Connect} and R_{Contact} resistances to be compensated for. This is accomplished by employing voltage sense electrodes (in a

Table 1
Summary of experimental details

Component/condition	Detail	Source
Membrane electrode assembly	Nafion® 112, Toray™ gas diffusion layer (TGP-H-060), dimensions: 4 cm × 12 cm; 0.38 mg cm^{-2} Pt (cathode); 0.4 mg cm^{-2} Pt/0.2 mg cm^{-2} Ru (anode)	(MEA) Johnson Matthey, Sonning Common, UK; (Nafion®) DuPont, Fayetteville, NC; (Diffuser) Toray Industries, Chuo-ku, Tokyo
Gas humidification	Nafion™ moisture exchange column. Capable of 100% humidification over the range of flow rates used	Omnifit, Cambridge, UK; (Thermocirculator) Julabo V, Germany
Anode gas	Hydrogen (99.999%)	BOC, UK
Cathode gas	Air (99.997%)	BOC, UK
Mass flow controllers	EL-FLOW®	Bronkhorst, Netherlands
Temperature controller	PID temperature controller 4 W × 25 W	Micro-Infinity™, Newport Electronics, USA; Weller heating elements, Cooper Tools, Germany
Impedance analyzer	1260 impedance analyzer; 10 mV$_{RMS}$ perturbation at 5 kHz	Solartron, Farnborough, UK
Segmented current collector plate (printed circuit board—PCB)	Au plated electrodes; nickel underlayer; 0.2 mm feature resolution; PCB design using Seetrax Ranger XL	AVA electronics, Wickford, UK Seetrax CAE Ltd. UK
Anode current collector	Phenolic resin impregnated graphite—bubble tight, 1 mm pitch cross-flow	Le Carbone (Great Britain) Ltd., UK
Gasket	Syndev® Silicone sheeting (0.15 mm)	Synergy Devices Ltd., UK
Clamping	Torque wrench, tightened to 5 N m	BRITOOL ACT 70, UK

fashion analogous to a 4-probe resistance measurement), leaving R_{MEA} to constitute the resistance measured at the high frequency limit of the EIS response.

1.2. An analytical model of current density distribution

An elegant and simple analytical expression dependent on the stoichiometric coefficient and reaction exponent has been used by Kornyshev and Kulikovsky (KK) to describe the current distribution along a single channel under the assumptions of low membrane resistivity, and Tafel-like kinetics for the electrochemical reaction when the reaction exponent for reactant in the channel = 1 [45,46]:

$$c(z) = c^0\left(1 - \frac{1}{\lambda}\right)^{z/L} \tag{3}$$

$$j(z) = \bar{j}\left(-\lambda\,\ln\left(1 - \frac{1}{\lambda}\right)\right)\left(1 - \frac{1}{\lambda}\right)^{z/L} \tag{4}$$

where c^0 is the inlet concentration to the channel, λ the stoichiometric coefficient, z the position along the channel, L the length of the channel and $\bar{j}$ is the average current along the channel. This approach has been extended to account for the formation of S-shaped localised polarisation curves that we have observed experimentally [39,47] and predicted using numerical modelling [48].

This expression has been shown to follow the current distribution in fuel cells of the same type as described in this paper under well-humidified conditions in which the membrane resistivity remains low. The purpose of this paper is to extend the previous experimental approach to examine the effect of low humidity conditions on the local current density and local membrane resistivity. The results are also used to ascertain when the KK model is no longer sufficient to describe the current distribution.

2. Experimental

Table 1 summarises the experimental conditions used in this work, details not included in the table are entered in the text.

The localised conductivity measurements presented here were made using the same system as has been described previously [39]. This system uses a segmented current collector on the cathode side of the cell, with a common collector on the anode side. The segmented current collector is fabricated using printed circuit board (PCB) technology, similar to that used by Cleghorn et al. [32]. Each current collector is associated with its own load circuit and the cell is controlled in potentiostatic mode. Previous workers have used MEAs which are segmented; however, our approach allows the use of an unsegmented electrode in a configuration representative of that found in a conventional fuel cell. The anode current collector plate is designed with cross-flow geometry and the cathode uses a single linear channel, i.e. there is no serpentine flow-field on the cathode side. The single channel is 1 mm wide 1 mm deep and has a lead-in and lead-out section located in a non-catalysed part of the MEA. This ensures that the flow is fully established and laminar before it enters the catalysed part of the channel.

The current collector board is composed of 100 electrodes (50 each side of the linear flow channel) routed via plated through holes (PTH) to the opposite side of the board. Each current contact is 2 mm × 8 mm and there is a gap of 0.2 mm between each. In this study the contact electrodes are grouped together (five electrodes on either side of the channel) to make ten sets of contacts, each connected to a separate potentiostat circuit. The total length of the channel covered by the current contacts is 11 cm. Individual contacts have been collected together as described since only 10 electronic load circuits were available.

The method of making localised impedance measurements has been described in a previous work [40]. A dc potential representing the target cell voltage is summed with a small amplitude ac voltage signal from an impedance analyser, and applied to each of the potentiostat circuits simultaneously. The correspond-

ing current and potential signal from each potentiostat is then routed back via a multiplexer to the impedance analyser and measured sequentially. The consequence of this is that the entire cell is subject to the same ac stimulus, but each impedance measurement is confined to the area of contact. Impedance scans in the frequency range 10 kHz to 0.1 Hz were performed for individual segments over a range of operating conditions. It was found that in all cases the intercept with the real axis was close to 5 kHz. Hence in measurements of membrane conductivity, we utilise a small amplitude ac voltage signal of frequency 5 kHz and amplitude of 10 mV_{RMS}. The phase angle was found to always be in the range $\pm 5^{\circ}$.

Since the fuel cell is run under a variety of potential, temperature and humidification conditions it was important that the cell was well equilibrated. Changes in potential were noted to affect a change in current almost immediately while changes in the humidification level produced changes in the conductance response which stabilised in the order of 10 min. During the course of the experiment, a time of at least 15 min (after the cell had reached temperature) were allowed for the cell to reach equilibrium.

At the anode, the hydrogen was delivered using a cross-flow configuration (Fig. 2). This involved multiple parallel 1 mm × 1 mm channels (on a 2 mm pitch) machined into the anode graphite flow field orientated 90° to the single cathode channel. At either end of these anode channels, there was a large manifold area to allow pressure equalisation and to ensure that supply of hydrogen to the anode was uniform. Hydrogen was supplied at a flow rate of 50 sccm, both in the humidified and non-humidified cases. This represents a stoichiometry of more than 3.5 for the highest total current recorded. Since the experiment has been designed with a single channel flow-field at the cathode and over-stoichiometric cross-flow at the anode, variation in the current and conductivity is exclusively due to the single channel of the cathode (i.e. flow rate and internal humidification) and the bulk properties of the cell (i.e. operating potential and temperature).

Reactant gas humidification was performed using a Nafion™ moisture exchange column (Omnifit, Cambridge, UK). This device is capable of 100% humidification over the range of flow rates used. Deionised water is delivered to the humidification column at the same temperature as that of the cell using a thermocirculator bath.

Values of current and resistance are reported as area specific in units of $A\,cm^{-2}$ and $\Omega\,cm^2$, respectively. The area to which each localised absolute value of current and resistance is normalised corresponds to the area under the channel for that portion of the channel but does not take into account the area under the land. Since a certain amount of reactant diffusion will occur to catalyst sites laterally away from the channel area, values of current density reported will tend to be higher than they actually are; likewise resistance values will be reported to be smaller since the impedance measurement samples a larger area than the width of the channel. However, the purpose of this study is not to report de facto values of membrane resistance for comparison with other work, but to provide a relative (although reasonable) scale of the spatial variation for a particular MEA and fuel cell geometry.

3. Results and discussion

Making comparisons of fuel cell performance over a range of operating conditions (i.e. temperature, flow rate, humidification and electrical loading), each potentially having a coupled association, is complex. Considering that each measurement is not simply a bulk quantity and likely to vary spatially, and that membrane resistance and current density distribution are both considered, it is clear that deconvolution of all of the factors that determine the response is not trivial.

The operating conditions investigated were chosen so as to represent significantly different modes of operation of the fuel cell. By studying the effect of making major changes to the operating parameters, comparison of the measured responses is more distinct. Anode gas humidification was performed at

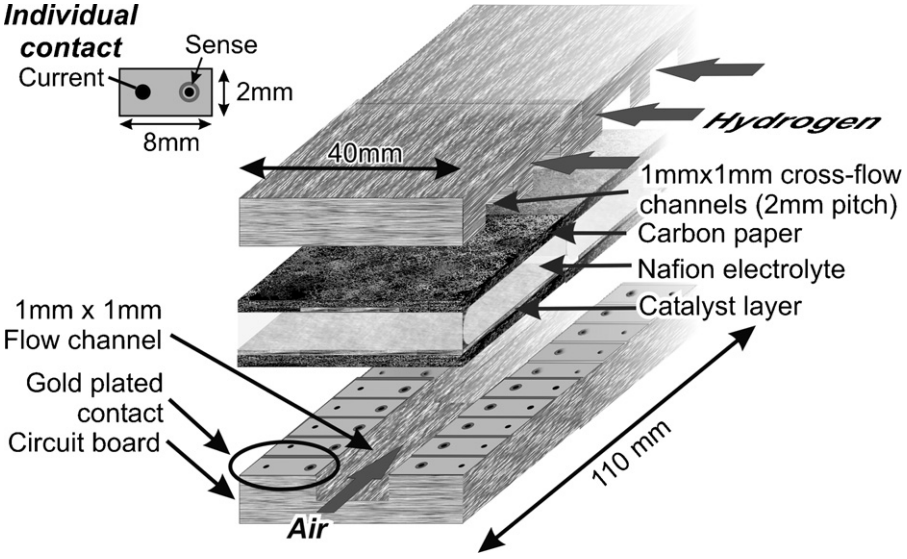

Fig. 2. Cartoon showing the cross-flow geometry used in the experimental apparatus.

values of 0 and 100% relative humidity; fuel cell temperatures of 30, 50 and 80 °C, representing the range of temperatures over which a PEFC would typically be operated; and operating potentials of 0.7 and 0.3 V were considered. A potential of 0.7 V was chosen to represent the typical operating voltage of a cell, whereas 0.3 V represents an inefficient mode of operation in a range characterised by mass transport limitation and high Ohmic losses. In addition, operating the cell at 0.3 V allows study of the effect of higher currents and is more likely to lead to inhomogeneous current distribution along the channel due to consumption of reactant and electrode flooding. Although such a condition would not be imposed intentionally on the system for an extended period of time, during periods of high load (such as vehicle acceleration) maximum power is required which corresponds to this regime of operation. The 0.3 V loading case should therefore be considered as a transitory or improperly regulated state.

The air flow rates studied were chosen to represent three different modes of operation, as experienced on the length scale of the flow channel used; at 10 sccm (average flow velocity 16.7 cm s^{-1}) the cell is likely to exist in a regime of reactant limitation (as predicted by the KK model) and to display signs of oxidant starvation along the length of the channel; at 100 sccm (average flow velocity 167 cm s^{-1}) the cell will not be subject to a significant concentration overpotential and at 500 sccm (average flow velocity 833 cm s^{-1}) a dehydrating effect on the electrolyte may result if proper water management cannot be maintained.

It is important to appreciate that the reactant-to-current stoichiometry imposed in these experiments should not be considered in the conventional sense. This is because the single channel studied is only one tenth to one twentieth the length of a typical channel in a fuel cell flow field—it thus represents a sub-section of a larger flow-field. In the case of the high air flow rate for example, a stoichiometry of over 50 may be experienced, which would never be imposed in a practical fuel cell. However, such a flow rate may be required in order to satisfy a larger fuel cell; this flow rate and gas composition will therefore be experienced at the start of a full flow-field. Likewise, a stoichiometry close to 1 results from the low air flow rate used to simulate reactant depletion (resulting in fuel cell starvation), a phenomenon that is more likely to occur at the end of a full flow-field.

The effect of hydration levels was studied by controlling the relative humidity of the anode and cathode reactant feed. Running the anode *and* cathode humidified at a cell temperature of 30 °C resulted in unstable operation of the cell due to flooding. Running the cell at 80 °C with no humidification at the anode or cathode resulted in deactivation of the cell due to membrane dehydration (corresponding to a total current of less than 10% of that obtained under properly humidified conditions). Neither of these modes of operation are considered further; however, humidification conditions within these extremes are presented.

The localised current and electrolyte resistance distribution at 30 and 80 °C are shown in Figs. 3 and 4, respectively. Measurements were also made at 50 °C; however, with the exception of slightly higher performance, similar features as for operation at 30 °C were observed. In addition to the experimentally measured values, the current density distribution prediction based on the KK model is also shown; linear regression fits to the electrolyte resistance data are added to illustrate the general trend alone the channel.

3.1. Current density distribution

At 30 °C (Fig. 3) the current and electrolyte resistance distribution remain relatively uniform across the range of conditions studied, with the exception of the low potential/low-flow case, where a current decay along the channel is observed. In all cases the KK model adequately describes the current distribution. If the fuel cell is operating in a regime in which current density is limited by oxygen partial pressure, localised current density measurements provide a map of those locations that are starved of oxygen. An example of current degradation due to reactant depletion can be seen in Fig. 3(b) where the current decreases to close to zero towards the end of the channel due to depletion of all of the available oxygen in the feed. Reactant depletion can occur via several mechanisms, these include: upstream utilisation of oxygen leaving the downstream channel devoid of reactant; blockage of a flow-field channel; poor flow-field design not allowing reactant access to the electrode or not allowing adequate removal of product water; a sudden increase in load may exhaust the reactant present and not be replenished until the supply has had a chance to respond.

There are several consequences of complete reactant consumption. The most obvious is that the current in that area of the fuel cell will fall to zero and that area of catalyst will be effectively redundant. If there is insufficient oxygen to sustain the locally imposed current passing through a region of a cell in a stack, the local reaction will switch to hydrogen evolution on the cathode. As well as lowering the potential of the cell, this presents an obvious safety risk. This process may also lead to damage to the cathode or anode electrocatalysts.

For each operating condition, once the system has reached equilibrium, the variation in the current measured from each point is of the order of the size of the data point shown. It should be noted that it is often seen that incongruent response is observed for the two end contacts compared to the rest of the current collection points. It is difficult to say if this is a consequence of genuinely different performance of the fuel cell at the channel ends, or a manifestation of a different current collection profile for the end contacts.

At 80 °C (Fig. 4), current and resistance distribution varies considerably more across all ranges of conditions studied. However, the KK model shows good correlation to the localised current density measurements with a couple of notable exceptions (Fig. 4(d and j)) which will be addressed below. The agreement between experiment and theory across such a wide range of operating conditions provides a strong endorsement for the analytical approach adopted by Kulikovsky and Kornyshev, showing that cumbersome numerical simulations with many fitting parameters are not necessarily required in order to predict current density distribution.

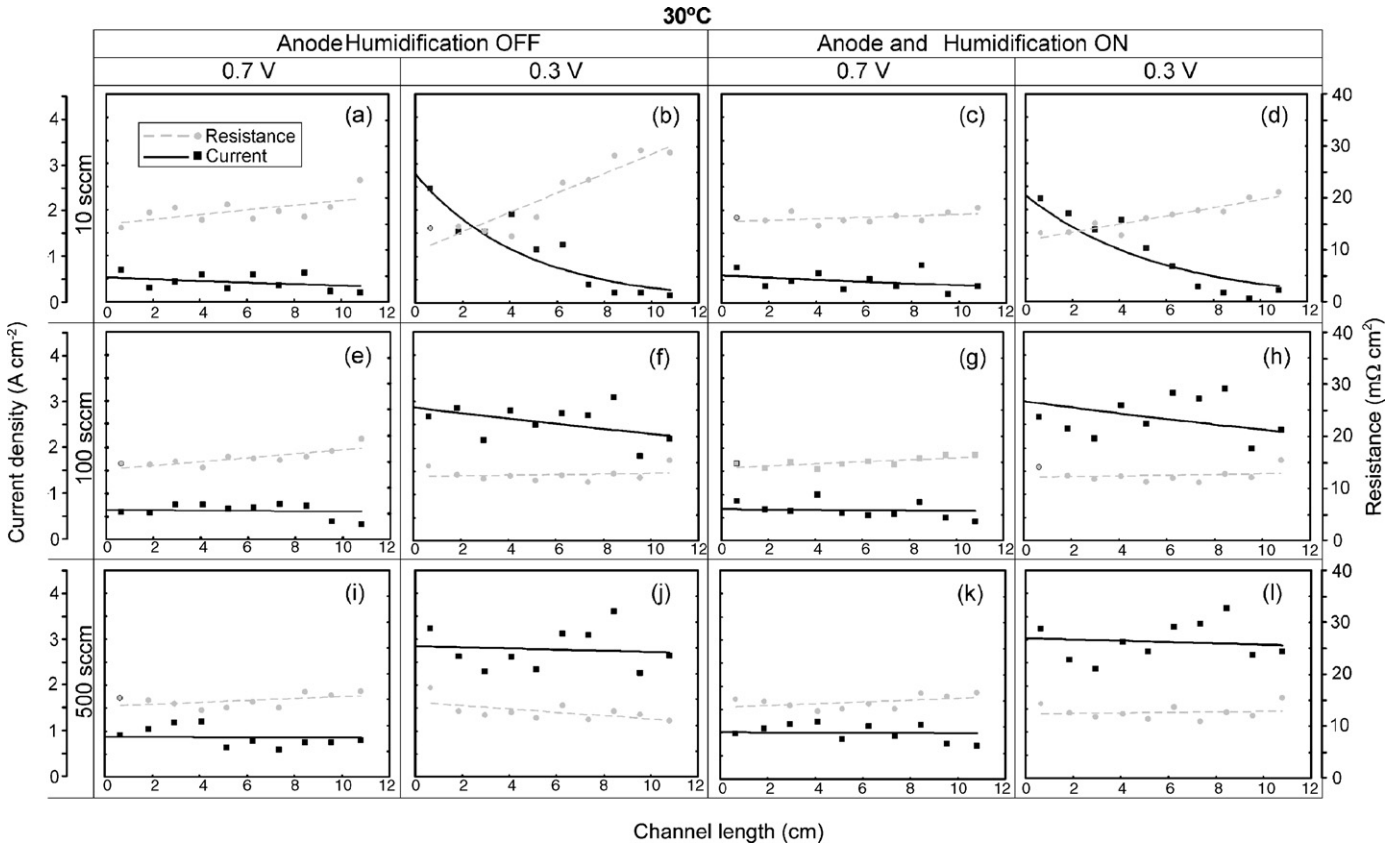

Fig. 3. Current and electrolyte resistance distribution profiles for operation at 30 °C.

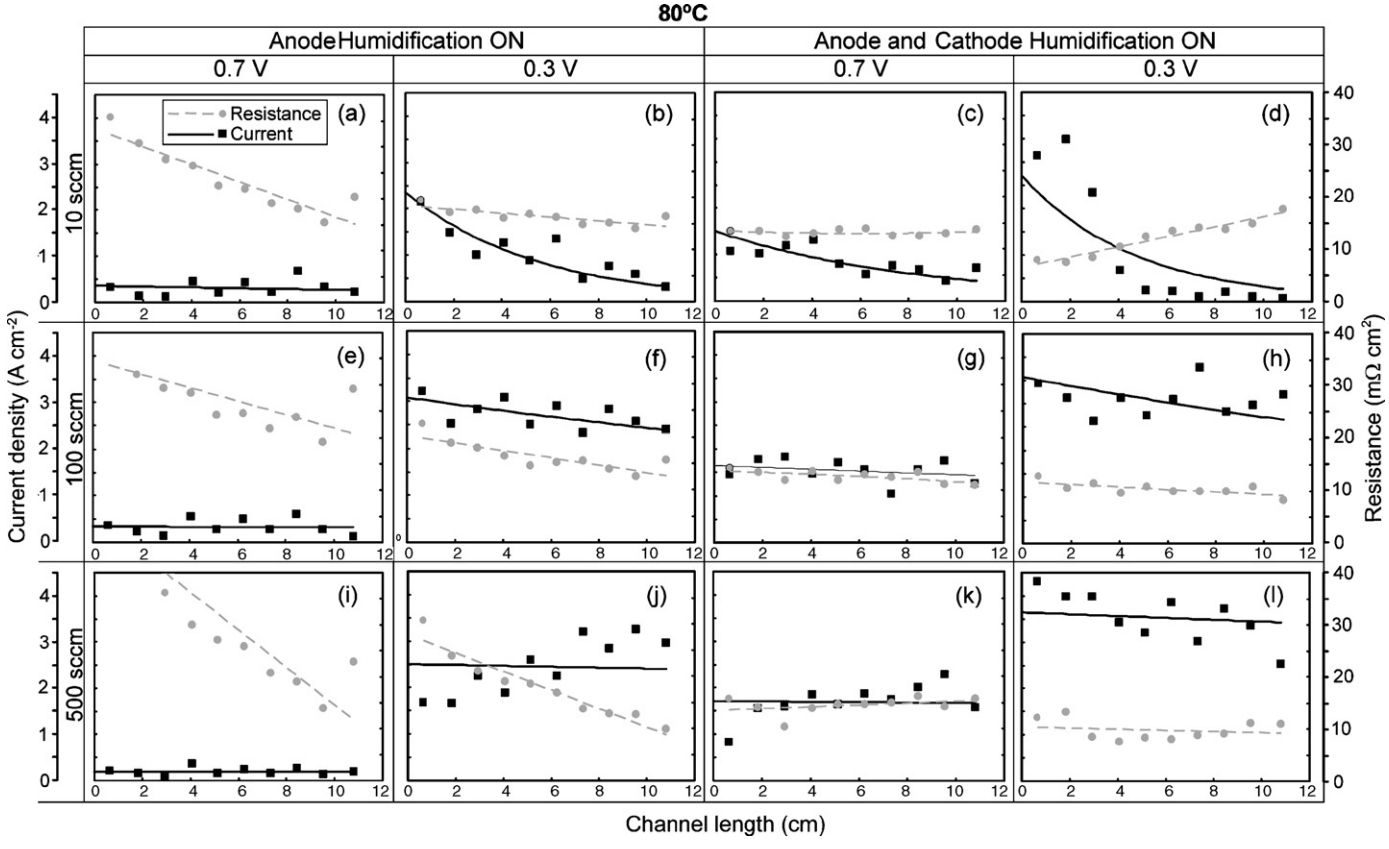

Fig. 4. Current and electrolyte resistance distribution profiles for operation at 80 °C.

Distinct from the fuel limiting case, current density distribution may also be affected by factors such as CO poisoning distribution [41], pore flooding or dehydration of the electrolyte membrane. In the case of electrolyte dehydration, the ability to make localised resistance measurements allows this effect to be monitored. Since the KK model does not consider spatial variation in electrolyte resistance, localised resistance measurements can be used to account for deviation between model and experiment due to this property.

3.2. Electrolyte resistance distribution

There is a range of behaviour in the resistance distributions measured at 30 and 80 °C. At 30 °C the resistance at the start of the channel is approximately the same in all cases, whereas at 80 °C there is a high degree of variability because of the greater difficulty in achieving water balance between the gas streams and the membrane. At higher temperature, membrane resistance almost always falls or is unchanging along the channel whereas at lower temperature it may increase with position along the channel.

3.2.1. Correlation between current density and electrolyte resistance

The relationship between membrane resistance and current density might be expected to be simple. All else being equal, a decrease in resistance is likely to result in an increase in current. However, the results show that the decrease in reactant concentration modulates this effect and can result in a variety of current and resistance distributions. Since water content in the electrolyte is a function of current density (due to water generated at the cathode and electro-osmotic drag), the two quantities are coupled such that under certain conditions, current density influences membrane resistance. An example of the latter is illustrated by the correlation between local current density and membrane resistance when the cell is run under conditions of reactant limitation, as seen in Fig. 3(b and d), for operation at 30 °C. For these two cases the current distribution is quite similar, with the membrane resistance at the beginning of the channel equal. However, the localised membrane resistance grows much quicker when neither of the reactant gases are humidified (Fig. 3(b)). Indeed, the resistance increases by 100% in this case whereas it only increases by about 50% when the anode gas is humidified. The correlation between the current density distribution and the KK function shows that it is not the resistance which is determining the current distribution but vice versa. Hence using the KK model it is possible to deconvolute the cause and effect of reactant utilisation on current and conductivity distribution.

Several studies have looked at the relationship between current density and membrane conductivity. Büchi et al. measured an *increase* in membrane resistance with current density (above 0.5 A cm^{-2}), the extent of this increase being more pronounced at lower temperatures [21]. Such a phenomenon has also been predicted from modelling [49]. The reasoning for this is that higher current density causes an increase in the net water flux from anode to cathode due to electro-osmotic drag. This dehydrates the anode, leading to an increase in membrane resistance. The membrane used in the Büchi study was the relatively thick Nafion™ N117 (nominal thickness 178 μm). This membrane thickness is preferred for use in the direct methanol fuel cell (DMFC), due to reduced permeation of methanol. However, PEFCs operating on hydrogen operate better with thinner membranes such as N112 (nominal thickness 50 μm) used in this study. This is because a thinner substance will exhibit a lower ionic resistance and enhanced back diffusion of water from the cathode to the anode. Studies comparing membrane resistance with current density for different membrane thicknesses show that an increase in resistance with current density is only observed for thicker membranes [28,30,50]. In the case of N112, current densities as high as 2 A cm^{-2} showed no increase in membrane resistance [30]. However, a *decrease* in membrane resistance with *increased* current density has been described by Watanabe et al. for a 57 μm thick Nafion® membrane [51]. They attribute the decrease in resistance at higher current densities (greater than 100 mA cm^{-2}) to the production of water at the cathode, back diffusing and hydrating the membrane. Likewise, the increase in electrolyte resistance with decreasing current density seen in this study is attributed to reduced water back diffusion. This effect is heightened towards the end of the channel where currents are small due to the low concentration of reactants. A further effect is that of anode humidification – it can be seen that water transported across the membrane via the electro-osmotic mechanism decreases the severity of the resistance increase when the anode gas is humidified – this leads to a less severe increase in membrane resistance with position, Fig. 3(d).

3.2.2. Membrane dehydration

Fig. 5 shows how the cell temperature and humidification level affects the average cell current and electrolyte resistance at a flow rate of 100 sccm. The intermediate flow rate is chosen to compare the bulk fuel cell response since this has the minimum spatial variation in current density and membrane resistance compared to the high and low flow rate cases. Under the conditions chosen for these experiments, the current distribution along the channel is relatively small, decreasing by no more than 20% along the length of the channel. Nonetheless the level of humidification still plays a significant role in determining performance, and this effect is made more apparent at elevated temperatures. At the two lower temperatures (30 and 50 °C) there is no significant improvement conferred by hydrating the anode stream, this is to be expected since below ca. 50 °C membrane conductivity has been shown to be approximately temperature invariant [3]; however, at 80 °C the loss in performance when running on dry anode and cathode feed is severe. The higher temperature also shows the need for cathode feed humidification in order to take advantage of the improved conductivity of the electrolyte at higher cell operating temperature.

Although the KK model is successful at predicting the current distribution for the majority of cases, there are conditions under which a current *increase* is recorded along the channel (e.g. Fig. 4(j)). Such effects occur at high flow rates and temperatures. Fig. 6 shows how increasing temperature affects the current and

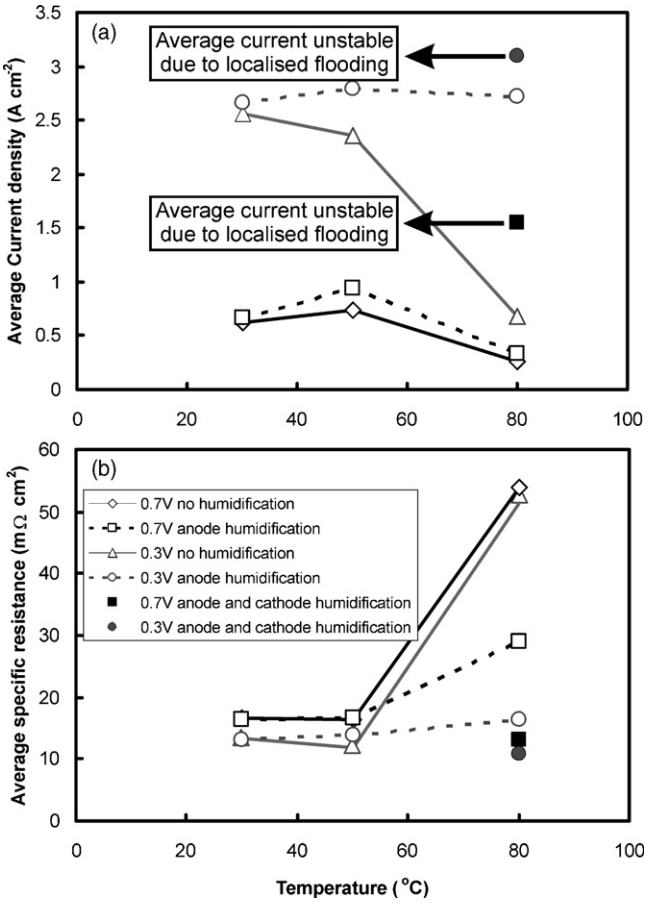

Fig. 5. Average cell current (a) and resistance (b) with temperature and humidification conditions for the cell operated at 100 sccm.

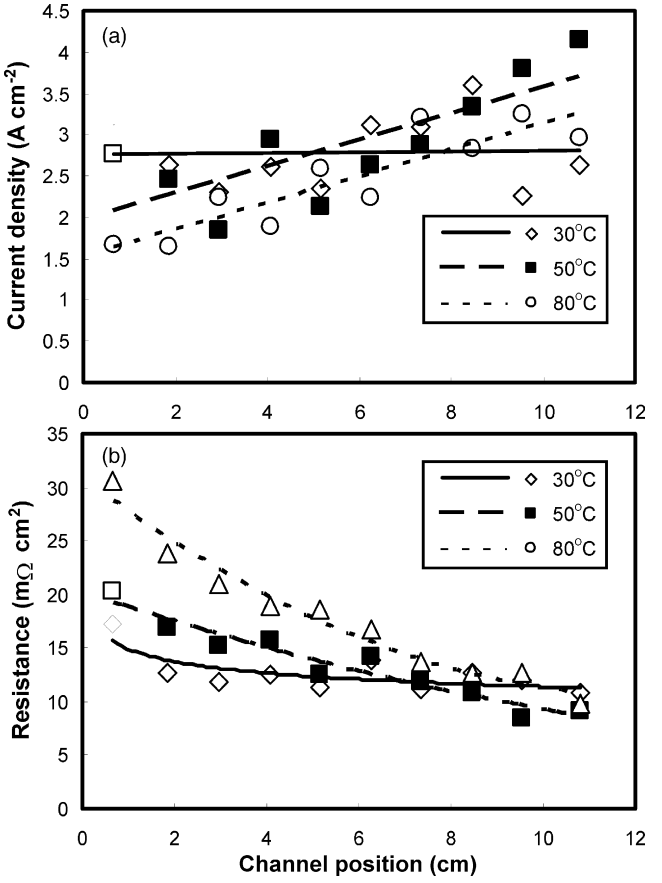

Fig. 6. Current (a) and resistance (b) distribution profiles at varying temperature and a flow rate of 500 sccm.

resistance distribution at a flow rate of 500 sccm. There is a clear trend in the electrolyte resistance distribution that shows that increasing temperature increases the electrolyte resistance at the start of the channel. At the end of the channel at all temperatures, the resistivity reaches a constant value.

Variation of resistivity with position has been predicted in modelling studies [16,52] and measured experimentally for a full flow-field by Cleghorn et al. who attribute it to internal humidification [32]. Sridhar et al. [53] found that the water pick-up by reactant gas increases significantly with temperature due to the elevated dew point; and that at low temperatures, increase in the rate of water pick-up with increased flow rate is not appreciable, as observed here.

The effect of membrane dehydration and internal humidification explains these results well. If the reactant gas enters the channel dry, then the low partial pressure of water at the start of the channel will lead to a greater transfer of water from the membrane material to the gas stream. This will have a dehydrating effect on the electrolyte, since there will be less water available to diffuse back through the membrane, and resistivity will be high. As the gas flows along the channel the water partial pressure increases, and the amount of membrane dehydration diminishes, manifest by a decrease in resistance. As the gas in the channel becomes humidified, it serves to hydrate the membrane in the same way as external humidification.

3.3. Activation of MEAs using localised conduction

After MEA manufacture, the polymer electrolyte is typically not in its optimal operating state for proper performance in a fuel cell. Furthermore, the catalyst may also need to be treated to increase its utilisation [54]. The state of the membrane at beginning of operation will depend on the method of MEA manufacture and the conditions in which it has been stored before use. There are various methods used to condition new MEAs, these include thermal cycling under humidified conditions, operation at elevated temperatures and pressures [55,56] and performing repetitive load cycles until constant output is obtained. Gaseous hydrogen evolution at the electrode has been reported to improve performance by changing the porosity and tortuosity of the catalyst layer [57] and boiling and steaming the MEA before incorporating into the cell is sometimes used to improve performance by activating the catalyst. However, there is no set protocol for achieving ‘activation’ of a PEFC, and it remains an inconvenient and problematic issue.

It has been shown that for the type of MEA investigated in this study, there is an inverse correlation between current density and electrolyte resistance; low current density due to reactant depletion leading to increase in electrolyte resistance. Hence maintaining local generation of water is crucial in maintaining the membrane in a well-hydrated state. This suggests that imposing high current density through an MEA may facilitate its

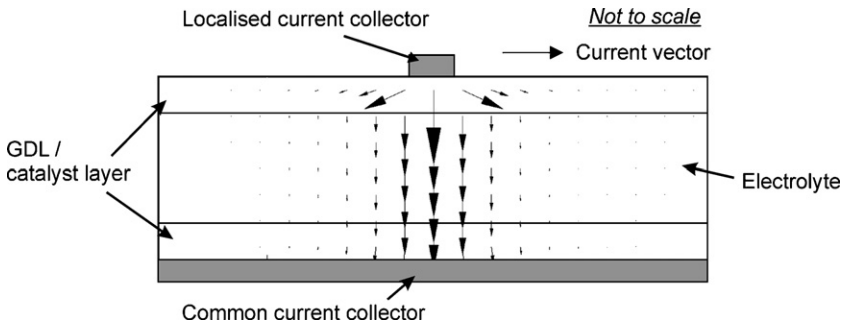

Fig. 7. Illustration of how localised current conduction results in a higher localised ionic current in the membrane electrolyte.

hydration, and lead to a membrane with low resistivity. This is often difficult to perform with normal fuel cell test rigs, as very high current densities (and concomitant reactant flows) may be required to achieve good hydration. A feature of the localised current mapping instrumentation used in this investigation is that it is possible to force current generated by reaction to occur within a controlled localised region in the fuel cell i.e. by using individual contacts to conduct the current—all of the reaction occurs in a region localised by one of the current collecting contacts; an illustration of how this happens is shown in Fig. 7. It is important to note that because the individual current contacts are driven in constant potential mode, it is not possible to have local reversal of the cell potential. Were such reversal to occur (as it might in a real fuel cell operated at high constant currents), local degradation of the catalyst or MEA may occur.

In order to test the assertion that imposed localised current can be used to hydrate membrane and ionomer in the catalyst layer, 'activation' of a previously unused MEA was attempted. It is often found that MEAs perform poorly during initial stages of operation, exhibiting highly varied response until the component is properly conditioned. Fig. 8 compares the current distribution measured for a previously unused MEA upon initial operation, and also after the entire fuel cell was cycled through varying degrees of loading and after three cycles of the "imposed localised current" method. It can be seen that initial operation of the virgin MEA results in a low current density across the extent of the cell. After cycling the whole-cell between a potential of 0.8 and 0.2 V ten times (resulting in a maximum current density of 1 A cm^{-2}—channel area specific) and taking 20 min, the current density was improved by a factor of two to a value of ~0.75 A cm^{-2} at a cell potential of 0.3 V. However, subjecting the cell to three cycles of localised conduction (10 s at each local point with a maximum channel area specific current density of 13 A cm^{-2} determined by the upper current limit of each potentiostat), taking a total of 5 min, the cell was found to exhibit a stable current density distribution with an average current density of ~2 A cm^{-2} more than five times higher than initially seen for this MEA. The method was generally found to be most effective at a cell temperature around 50 °C and with humidified anode gas. Although not a guaranteed method of achieving a certain desired fuel cell performance, localised conduction has hastened the achievement of stable operation of virgin MEAs during the course of this study. Such a procedure seems to be a much swifter method for achieving stable and satisfactory performance when conditioning fresh MEAs.

The activation process is thought to occur because of accelerated hydration of the membrane and ionomer in the catalyst layer caused by forced localised conduction of the available current generated. The localised current and membrane resistance measurements presented herein have shown that an increase in the current passing through the membrane results in a lower membrane resistance (for the N112 used in this investigation) due to the hydrating effect of electro-osmotic drag and product water formation. So, by artificially increasing the current at a certain point, hydration of the membrane should occur with a corresponding increase in conductance. However, it was found that for an MEA that had been in constant operation for some time, changes in reactant hydration, temperature and current density

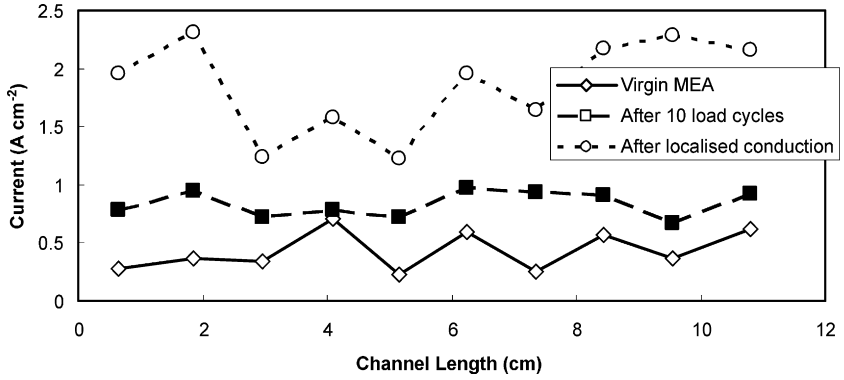

Fig. 8. Current distribution for a previously unused MEA and that after load cycling and localised conduction (50 °C, anode humidified, 0.3 V, 100 sccm).

caused a change in the conductivity of the membrane (indicative of the level of hydration) over a period of only seconds or minutes. For a previously unused MEA the conditioning period is typically much longer. This suggests that the initial hydration process has an activation barrier to overcome. This may be due to the formation of percolation networks for protons crossing the membrane material [58].

Although the localised conduction method may not be easily applicable in a practical fuel cell, it may be possible to implement this process to precondition the MEAs before their manufacture into a stack.

4. Conclusion

Localised current density and electrolyte resistance mapping has been reported for a single channel cathode flow-field in a fuel cell operating at varying air flow rate, humidification, cell temperature and voltage conditions. Current density distribution measurements are compared with an analytical model developed by Kulikovsky and Kornyshev. Good agreement is observed between model and measurement across a wide range of operating conditions. However, under certain conditions an increase in current density along the length of the channel is observed, which is not accounted for in the model. Localised electrolyte resistance measurements revealed the current increase phenomenon to be a consequence of electrolyte drying, exacerbated by high temperature and flow rates.

These measurements have provided insight into the variation in membrane hydration and the effect that different operating conditions have upon it. Some of our observations qualitatively endorse the findings of Cleghorn et al. [32], such as evidence of internal humidification. However, a disparity exists in the correlation between current and electrolyte resistance; the previous study reports an increase in resistance at higher current density, whereas the results presented here show no such connection. In the case of reactant depletion along the channel, resulting in very low currents, resistance is actually seen to *increase*. We consider differences between the two studies to be due to the thinner membrane used in this work, so rendering the resistance of the electrolyte much less sensitive to operating parameters; whereas the thicker N117 is known to vary significantly with changes in current density, humidification and temperature [28].

In terms of water management, running the cell under co-flow and counter-flow conditions [7,11,12,18] as well as dead-ended parallel geometry (interdigitated) [59] are predicted to result in more profound variations in current and membrane resistance. Despite N112 being robust in terms of its ability to operate well under a range of conditions, this technique was sensitive enough to discern some marked variations in spatial membrane resistance.

When interpreting spatially varying measurements, further factors that should be considered including the effect of pore flooding; condensation of water in the channel; localised temperature variation; lateral flow of ionic current and the complex issue of ‘membrane memory’.

It should be appreciated that the conditions of operation chosen for this study were intended to represent a broad range with extremes, such that differences in current density and resistance are discernable over a relatively short channel length (i.e. 11 cm). If the length of a channel is notionally extended to be of the order of length used in a full flow-field, then it can be expected that many of the features exhibited here, will be exacerbated over a longer channel length.

Acknowledgments

We would like to thank Johnson Matthey for providing MEAs and Simon Turner for help with fuel cell construction. This project was funded by the United Kingdom EPSRC under grant GR/M 73552.

References

[1] L. Carrette, K.A. Friedrich, U. Stimming, Chem. Phys. Chem. 1 (2000) 162–193.
[2] T.A. Zawodzinski, C. Derouin, S. Radzinski, R.J. Sherman, V.T. Smith, T.E. Springer, S. Gottesfeld, J. Electrochem. Soc. 140 (1993) 1041–1047.
[3] T.A. Zawodzinski, T.E. Springer, J. Davey, R. Jestel, C. Lopez, J. Valero, S. Gottesfeld, J. Electrochem. Soc. 140 (1993) 1981–1985.
[4] R.S. Yeo, J. Electrochem. Soc. 130 (1983) 533–538.
[5] G. Pourcelly, A. Oikonomou, C. Gavach, H.D. Hurwitz, J. Electroanal. Chem. 287 (1990) 43–59.
[6] T. Okada, G. Xie, O. Gorseth, S. Kjelstrup, N. Nakamura, T. Arimura, Electrochim. Acta 43 (1998) 3741–3747.
[7] J.S. Yi, Y.V. Nguyen, J. Electrochem. Soc. 145 (1998) 1149–1159.
[8] T.V. Nguyen, R.E. White, J. Electrochem. Soc. 140 (1993) 2178–2186.
[9] X. Ren, S. Gottesfeld, J. Electrochem. Soc. 148 (2001) A87–A93.
[10] D.M. Bernardi, M.W. Verbrugge, J. Electrochem. Soc. 139 (1992) 2477–2491.
[11] S. Dutta, S. Shimpalee, J.W. Van Zee, J. Appl. Electrochem. 30 (2000) 135–146.
[12] D. Singh, D.M. Lu, N. Djilali, Int. J. Eng. Sci. 37 (1999) 431–452.
[13] G.J.M. Janssen, J. Electrochem. Soc. 148 (2001) A1313–A1323.
[14] G.J.M. Janssen, M.L. Overvelde, J. Power Sources 101 (2001) 117–125.
[15] H. Nishikawa, R. Kurihara, S. Sukemori, T. Sugawara, H. Kobayasi, S. Abe, T. Aoki, Y. Ogami, A. Matsunaga, J. Power Sources 155 (2006) 213–218.
[16] T.F. Fuller, J. Newman, J. Electrochem. Soc. 140 (1993) 1218–1225.
[17] T. Okada, G. Xie, Y. Tanabe, J. Electroanal. Chem. 413 (1996) 49–65.
[18] H.P.L.H. van Bussel, F.G.H. Koene, R.K.A.M. Mallant, J. Power Sources 71 (1998) 218–222.
[19] G. Maggio, V. Recupero, L. Pino, J. Power Sources 101 (2001) 275–286.
[20] N. Yoshida, T. Ishisaki, A. Watakabe, M. Yoshitake, Electrochim. Acta 43 (1998) 3749–3754.
[21] F.N. Buchi, G.G. Scherer, J. Electroanal. Chem. 404 (1996) 37–43.
[22] A.V. Anantaraman, C.L. Gardner, J. Electroanal. Chem. 414 (1996) 115–120.
[23] S. Nouri, L. Dammak, G. Bulvestre, B. Auclair, Eur. Polym. J. 38 (2002) 1907–1913.
[24] M. Verbrugge, R. Hill, J. Electrochem. Soc. 137 (1990) 3770–3777.
[25] M. Verbrugge, E.W. Schneider, R.S. Conell, R. Hill, J. Electrochem. Soc. 139 (1992) 3421–3428.
[26] T.E. Springer, T.A. Zawodzinski, M.S. Wilson, S. Gottesfeld, J. Electrochem. Soc. 143 (1996) 587–599.
[27] M. Ciureanu, R. Roberge, J. Phys. Chem. B. 105 (2001) 3531–3539.
[28] T.J.P. Freire, E.R. Gonzalez, J. Electroanal. Chem. 503 (2001) 57–68.
[29] Y. Sone, P. Ekdunge, D. Simonsson, J. Electrochem. Soc. 143 (1996) 1254–1259.
[30] S. Slade, S.A. Campbell, T.R. Ralph, F.C. Walsh, J. Electrochem. Soc. 149 (2002) A1556–A1564.
[31] J.J.T.T. Vermeijlen, L.J.J. Janssen, A.J. Geurts, G.C. Van Haastrecht, J. Appl. Electrochem. 25 (1995) 1122–1127.

[32] S.J.C. Cleghorn, C.R. Derouin, M.S. Wilson, S. Gottesfeld, J. Appl. Electrochem. 28 (1998) 663–672.
[33] C.J. Brown, D. Pletcher, F.C. Walsh, J.K. Hammond, D. Robinson, J. Appl. Electrochem. 22 (1992) 613–619.
[34] J. Stumper, S.A. Campbell, D.P. Wilkinson, M.C. Johnson, M. Davis, Electrochim. Acta 43 (1998) 3773–3783.
[35] Ch. Wieser, A. Helmbold, E. Gülzow, J. Appl. Electrochem. 30 (2000) 803–807.
[36] M. Noponen, T. Mennola, M. Mikkola, T. Hottinen, P. Lund, J. Power Sources 106 (2002) 304–312.
[37] N. Rajalakshmi, M. Raja, K.S. Dhathathreyan, J. Power Sources 112 (2002) 331–336.
[38] M.M. Mench, C.Y.H. Wang, J. Electrochem. Soc. 150 (2003) A79–A85.
[39] D.J.L. Brett, S. Atkins, N.P. Brandon, V. Vesovic, N. Vasileiadis, A.R. Kucernak, Electrochem. Commun. 3 (2001) 628–632.
[40] D.J.L. Brett, S. Atkins, N.P. Brandon, V. Vesovic, N. Vasileiadis, A.R. Kucernak, Electrochem. Solid State Lett. 6 (2003) A63–A66.
[41] D.J.L. Brett, S. Atkins, N.P. Brandon, V. Vesovic, N. Vasileiadis, A.R. Kucernak, J. Power Sources 133 (2004) 205–213.
[42] D.J.L. Brett, P. Aguiar, N.P. Brandon, A.R. Kucernak, Int. J. Hydrogen Energy 32 (2007) 863–871.
[43] M. Noponen, T. Hottinen, T. Mennola, M. Mikkola, P. Lund, J. Appl. Electrochem. 32 (2002) 1081–1089.
[44] F.N. Büchi, G.G. Scherer, in: S. Gottesfeld, T.F. Fuller (Eds.), Proton Conducting Membrane Fuel Cells II, PV 98-27, The Electrochemical Society Proceedings Series, Pennington, NJ, 1998, p. 71.
[45] H. Dohle, A.A. Kornyshev, A.A. Kulikovsky, J. Mergel, D. Stolten, Electrochem. Commun. 3 (2001) 73–80.
[46] A.A. Kornyshev, A.A. Kulikovsky, Electrochim. Acta 46 (2001) 4389–4395.
[47] A.A. Kulikovsky, A. Kucernak, A.A. Kornyshev, Electrochim. Acta 50 (2005) 1323–1333.
[48] N. Vasileiadis, D.J.L. Brett, V. Vesovic, A.R. Kucernak, E. Fontes, N.P. Brandon, J. Fuel Cell Sci. Technol., in press.
[49] T.E. Springer, T.A. Zawodzinski, S. Gottesfeld, J. Electrochem. Soc. 138 (1991) 2334–2342.
[50] J.A. Kolde, B. Bahar, in: S. Gottesfeld, G. Halpert, A. Landgrebe (Eds.), Proton Conducting Membrane Fuel Cells, PV 95-23, The Electrochemical Society Proceedings Series, Pennington, NJ, 1995, p. 193.
[51] M. Watanabe, H. Igarashi, H. Uchida, F. Hirasawa, J. Electroanal. Chem. 399 (1995) 239–241.
[52] K. Dannenberg, P. Ekdunge, G. Lindburgh, J. Appl. Electrochem. 27 (2000) 1377–1387.
[53] P. Sridhar, R. Perumal, N. Rajalakshmi, M. Raja, K.S. Dhathathreyan, J. Power Sources 101 (2001) 72–78.
[54] Z. Qi, A. Kaufman, J. Power Sources 109 (2002) 227–229.
[55] Z. Qi, A. Kaufman, J. Power Sources 114 (2003) 21–31.
[56] Z. Qi, A. Kaufman, J. Power Sources 111 (2002) 181–184.
[57] C. He, Z. Qi, M. Hollett, A. Kaufmann, Electrochem. Solid-State Lett. 5 (2002) A138–A181.
[58] E. Spohr, P. Commer, A.A. Kornyshev, J. Phys. Chem. B 106 (2002) 10560–10569.
[59] A.S. Aricò, P. Cretì, V. Baglio, E. Modica, V. Antonucci, J. Power Sources 91 (2000) 202–209.